Structural and chemical changes in hardwood cell walls during early stages of flash pyrolysis

Jake K. Lindstrom[1,2], Chad A. Peterson[1,2], Peter N. Ciesielski[3],
John Ralph[4], Mingjie Chen[4], Joseph E. Jakes[5],
Patrick A. Johnston[2], Sean A. Rollag[6] and Robert C. Brown[1,2,6]*

[1]Department of Mechanical Engineering, Iowa State University, Ames, IA, United States, [2]Bioeconomy
Institute, Iowa State University, Ames, IA, United States, [3]Biosciences Center and National Bioenergy
Center, National Renewable Energy Laboratory, Golden, CO, United States, [4]Department of
Biochemistry, and the Department of Energy's Great Lakes Bioenergy Research Center, The Wisconsin
Energy Institute, University of Wisconsin-Madison, Madison, WI, United States, [5]Forest Biopolymers
Science and Engineering, USDA Forest Service, Forest Products Laboratory, Madison, WI, United States,
[6]Department of Chemical and Biological Engineering, Iowa State University, Ames, IA, United States
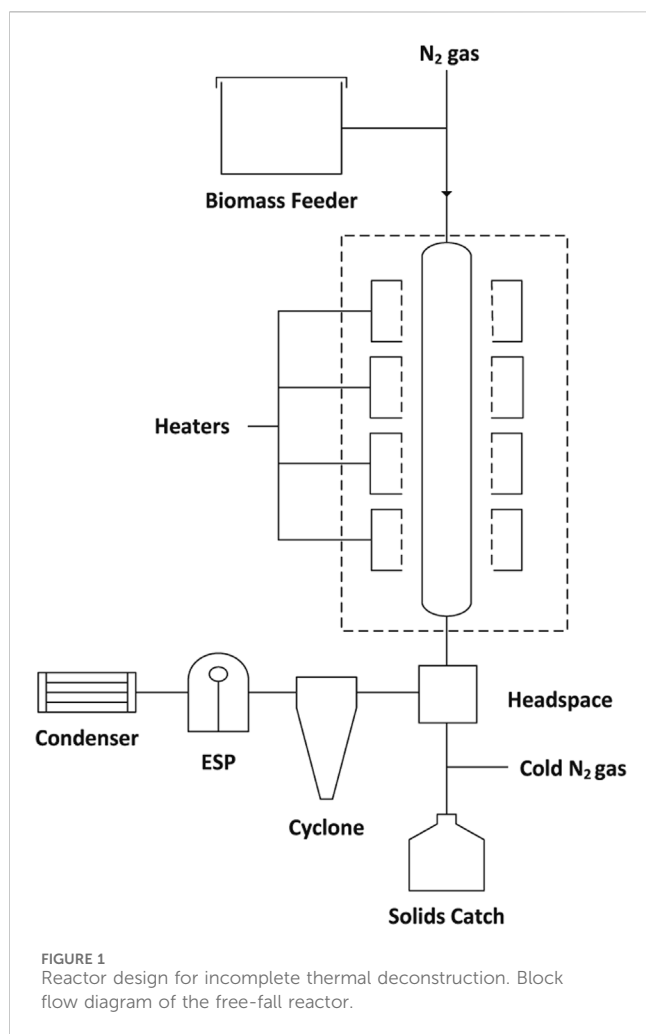
Volatile products from thermal decomposition of lignocellulosic biomass have
been well characterized, but the solid- and liquid-phase reactions during the
early stages of decomposition are largely unknown. Here the initial solid-phase
biomass thermal deconstruction reactions were analyzed *in situ* and with high
particle heating rates, delineating how these processes occur. A variety of
instrumentation was used to quantify the extent and relative rates of
deconstruction, demonstrating that biopolymers resist the thermally energetic
conditions to differing degrees, even when ensconced in biomass cell walls.
Hemicellulose and the more frangible lignin components decompose and
volatilize more readily than cellulose, which temporarily enriches biomass with
cellulose. These chemical changes manifest in larger cell wall structural and
mechanical property transformations. In all, this investigation concludes that
these solid-phase reactions strongly influence the production rates of volatile
species and will require additional study before these processes can be modeled
precisely to improve yields of desired product.

1 Introduction

Thermochemical processing, which employs thermal energy at elevated temperatures to achieve rapid deconstruction of feedstocks, is effective in converting recalcitrant lignocellulosic biomass into gaseous, liquid, and solid products Zhang et al. (2019). These thermally-driven processes include pyrolysis, Bridgwater, (2012) gasification, Sikarwar et al. (2016) combustion, Mandø, (2013) and solvent liquefaction Ghosh et al. (2019). Thermochemical processes have been exploited by humankind for thousands of years to convert coal and biomass into energy and chemical products, and yet the incipient reactions common to all four processes are poorly understood Lindstrom et al. (2019a). This limited understanding of condensed-phase reactions arises from two sources: the focus of most thermochemical processes is to produce volatile products; and it is notoriously difficult to interrogate the high temperature reactions within condensed-phase matter.

FIGURE 1
Reactor design for incomplete thermal deconstruction. Block flow diagram of the free-fall reactor.

FIGURE 2
Reactor yields from incomplete red oak thermal deconstruction. Product yield dependence on reactor temperature. Error indicated as standard error only for 450°C as this temperature was tested in duplicate.

Volatile products include hot flue gas from combustion, synthesis gas (syngas) from gasification, and bio-oil condensed from fast pyrolysis or solubilized during solvent liquefaction. For millennia, humans have used these products for heating, Gowlett, (2016) curing pottery, Gowlett, (2016) embalming Pharaohs, Koller et al. (2005) waterproofing ships, Evershed et al. (1985) as well as a plethora of other applications Breault, (2010); Lillebø et al. (2013); Shanks and Keeling, (2017); Iisa et al. (2018). Today, these products being evaluated for use as biofuel and biobased chemical precursors. Accordingly, researchers have focused on characterizing volatile products released from thermochemical processes, but this approach has created a substantial knowledge gap: condensed-phase reactions that precede volatile product formation Lindstrom et al. (2019a).

For several decades, researchers have recognized the importance of condensed-phase reactions in determining the outcome of thermochemical processes but have not had methodologies to interrogate the interior of hot, rapidly reacting biomass particles. Consequently, researchers have resorted to deducing reaction mechanisms from volatile products released from the condensed phase, which is frequently not time resolved. Several recent studies have leveraged innovative reactor designs to truncate rapid thermal deconstruction prematurely so that intermediate products can be analyzed; (Thompson et al., 2017; Zhu et al., 2017; Lindstrom et al.,
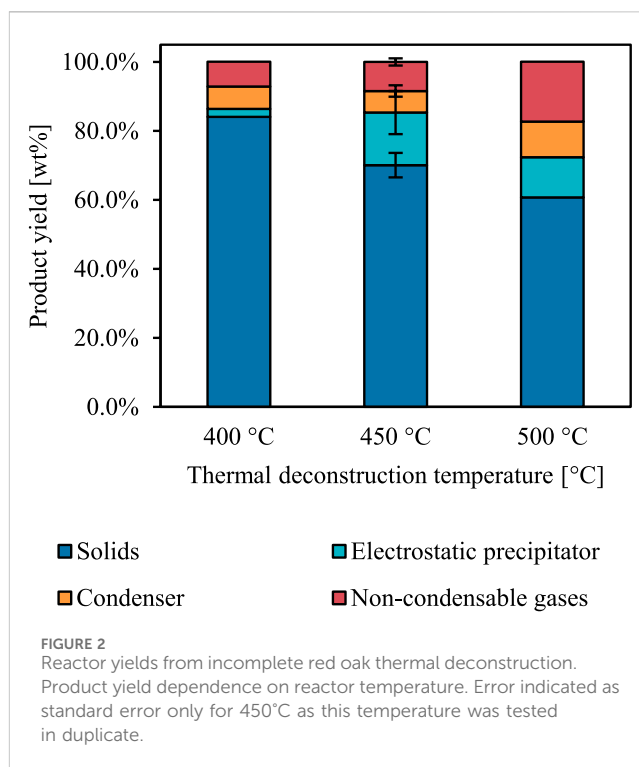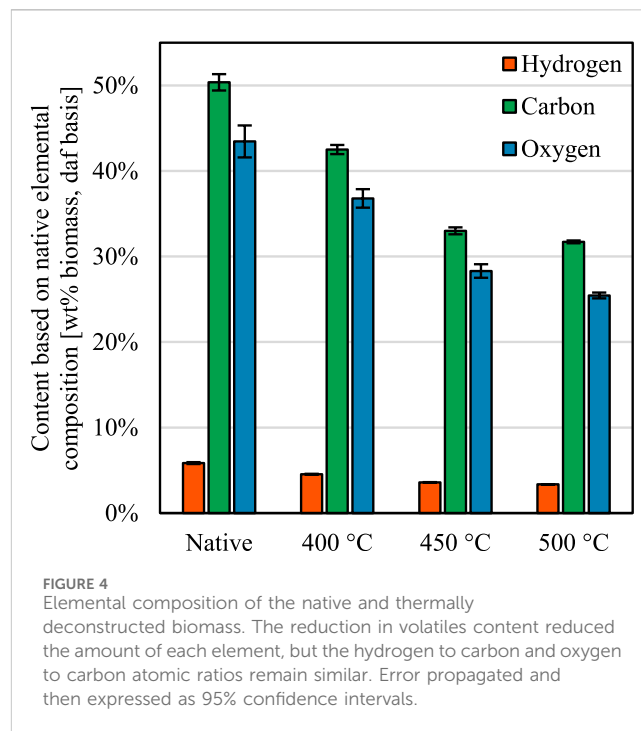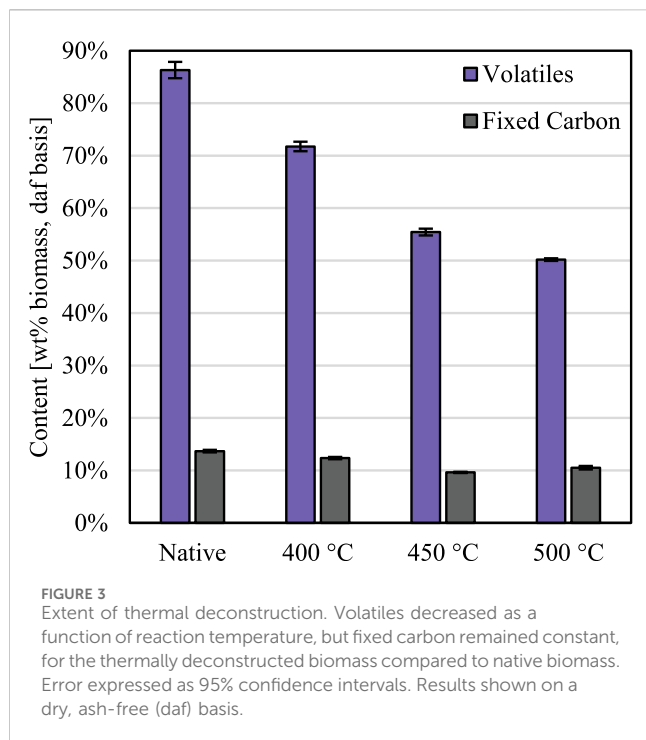
2019b); however, none of these efforts has investigated solid-phase reactions within lignocellulosic biomass.

Herein, the reactions occurring during rapid biomass thermal deconstruction were broadly analyzed. This investigation focuses on the early stages of thermochemical processing, before subsequent gas-phase reactions. By concentrating solely on the initial solid-phase reactions, these results and conclusions are applicable to most high temperature biomass thermochemical processing methodologies because they primarily differ in the extent and type of secondary gas-phase reactions Lindstrom et al. (2019a). An enhanced understanding of these initial reactions can inform subsequent modeling and related efforts to improve these processes.

2 Thermal deconstruction of biomass particles

So-called "truncated thermal deconstruction" experiments were performed on *Quercus rubra* (red oak) and extracted cellulose in a free-fall reactor (Figure 1) to produce partially-reacted solid particles (Figure 2). The red oak biomass was debarked and comminuted to particles ranging from 250–850 μm. These partially-reacted samples were subjected to offline analysis using a variety of sophisticated analytical methods to understand incipient reactions in the condensed phase. The continuously-fed biomass fibers (250–850 μm) and cellulose particles (50 μm) were entrained through the pre-heated reactor zone with nitrogen gas. After approximately 0.9 s of reaction time the exiting particles were quenched with cold nitrogen gas (approximately −196°C). The Supplemental Material presents additional free-fall modeling. Volatile products were condensed by an electrostatic precipitator

FIGURE 3
Extent of thermal deconstruction. Volatiles decreased as a function of reaction temperature, but fixed carbon remained constant, for the thermally deconstructed biomass compared to native biomass. Error expressed as 95% confidence intervals. Results shown on a dry, ash-free (daf) basis.

FIGURE 4
Elemental composition of the native and thermally deconstructed biomass. The reduction in volatiles content reduced the amount of each element, but the hydrogen to carbon and oxygen to carbon atomic ratios remain similar. Error propagated and then expressed as 95% confidence intervals.
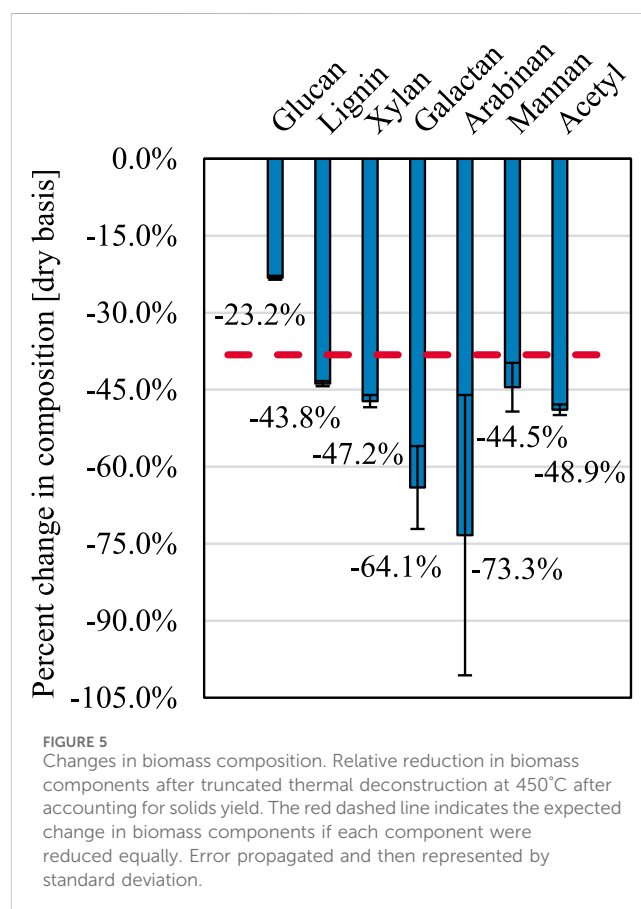
(ESP) followed by a water-cooled condenser. By performing experiments at three different reactor temperatures (375, 400, 450, 500°C), it was possible to examine the effect of temperature on product yields and biopolymer composition.
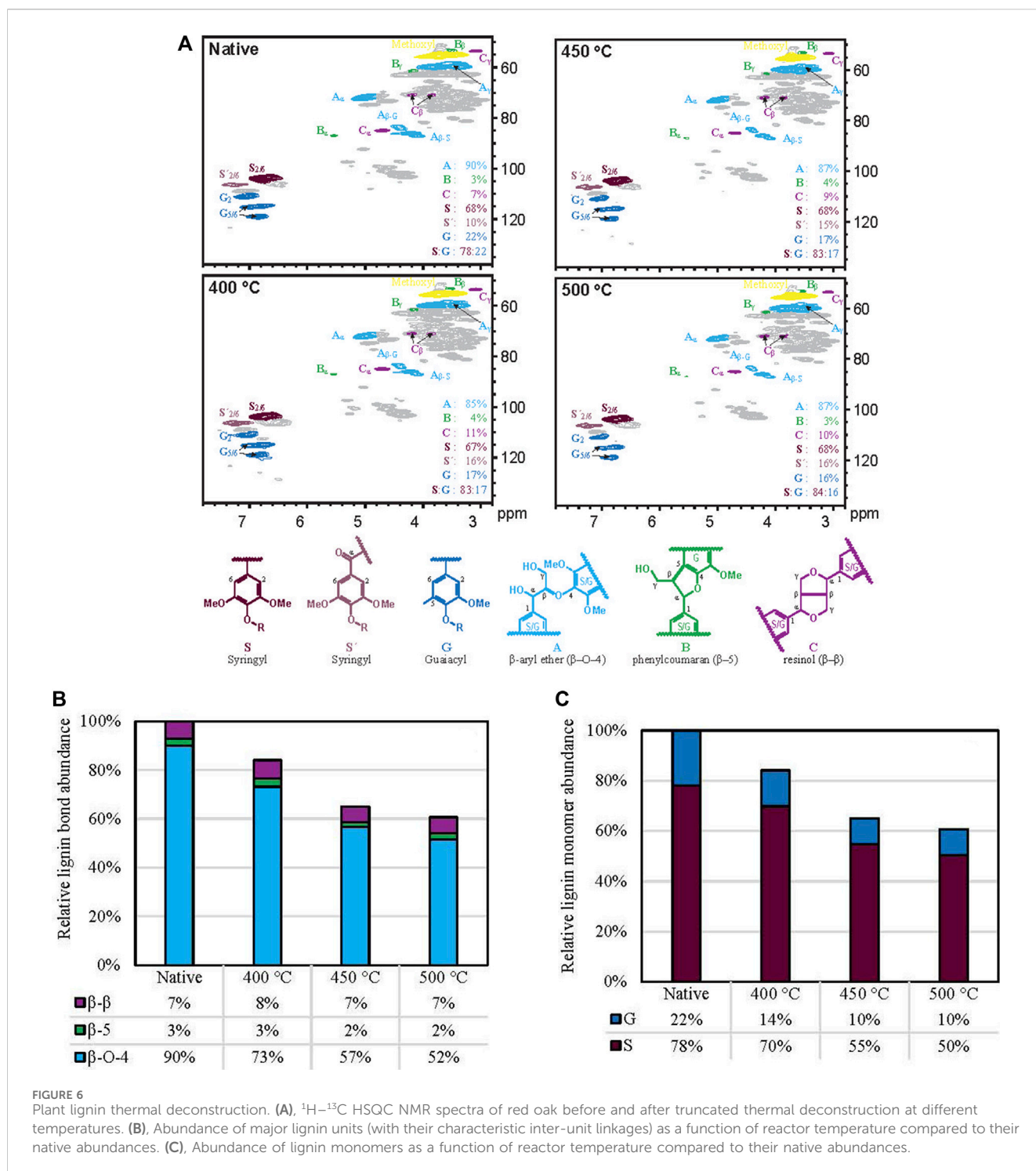
The ash, fixed carbon, and volatiles content of the red oak was measured both before partial thermal deconstruction (termed "native") and also after (labelled according to reactor temperature) to gauge the severity of reaction conditions (Figure 3). The volatiles content of the partially deconstructed red oak decreased with increasing reactor temperature compared to native red oak. However, under the most severe reactor conditions, the partially reacted red oak still retained 60% of its initial volatiles content, indicating that the biomass particles were only moderately degraded—a significant distinction between previous efforts to probe the early stages of thermal deconstruction.

3 Chemical deconstruction

To analyze basic chemical deconstruction trends, the elemental composition of native and partially deconstructed red oak was measured. These results reveal that rapid thermochemical processing deconstructs biomass differently than slower methods. In slow thermal deconstruction processes, such as torrefaction or slow pyrolysis, the hemicellulosic fraction of biomass degrades first, which lowers the atomic ratios of oxygen to carbon and hydrogen to carbon Tumuluru et al. (2011); Weber and Quicker, (2018); Lindstrom et al. (2019a). In the rapid thermochemical experiments, however, these ratios do not change significantly during the process (Figure 4), indicating that all biopolymers—both polysaccharides and lignin—degraded simultaneously during these truncated thermal deconstruction experiments.

FIGURE 5
Changes in biomass composition. Relative reduction in biomass components after truncated thermal deconstruction at 450°C after accounting for solids yield. The red dashed line indicates the expected change in biomass components if each component were reduced equally. Error propagated and then represented by standard deviation.
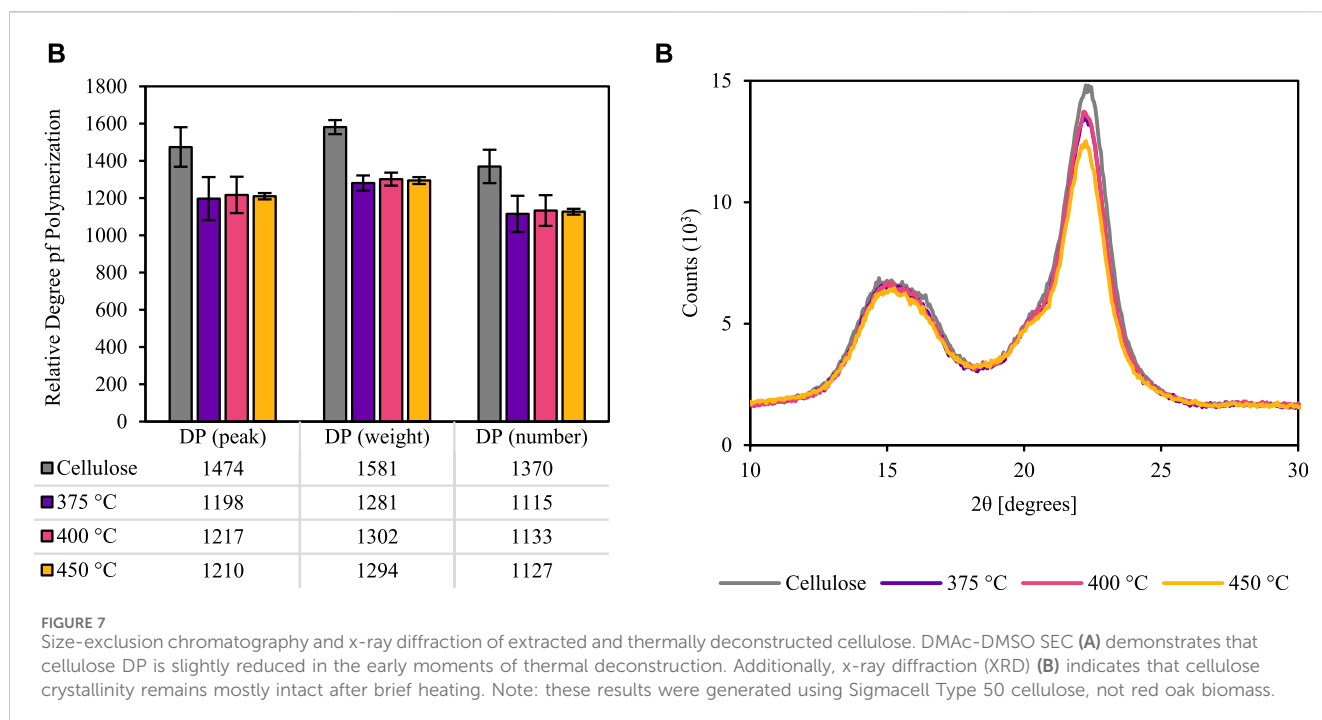
To investigate how each biopolymer degrades individually, the biomass composition was analyzed. Except for lignin, these experiments do not quantify biopolymers directly but measure sub-components that

FIGURE 6
Plant lignin thermal deconstruction. **(A)**, $^1H-^{13}C$ HSQC NMR spectra of red oak before and after truncated thermal deconstruction at different temperatures. **(B)**, Abundance of major lignin units (with their characteristic inter-unit linkages) as a function of reactor temperature compared to their native abundances. **(C)**, Abundance of lignin monomers as a function of reactor temperature compared to their native abundances.

reflect the amounts of biopolymers formed Sluiter et al. (2012). Cellulose is a polymer composed of glucose monomers; correspondingly glucan serves as a cellulose proxy; however, hemicellulose also contains some glucan, which slightly obscures this glucan-cellulose surrogacy. In addition to glucan, hemicelluloses are composed of xylan, galactan, mannan, and arabinan as well as hexuronic acids and may be decorated with pendant acetyl groups Holtzapple and Caballero, (2003). In lignocellulosic biomass, these monosaccharides and the acetyl moiety are only derived from

hemicelluloses, so they serve as hemicellulose indicators. While imperfect, this methodology allows investigation of changes in biopolymer composition during thermal deconstruction.

Figure 5 indicates the extent of solid-phase biopolymer deconstruction. Cellulose (composed of glucose monomers) is more resistant to thermal deconstruction than either lignin or hemicelluloses. Thus, during thermal deconstruction, biomass is enriched temporarily with cellulose as the relative composition of cellulose rises due to the disproportionate volatilization rates of the

FIGURE 7
Size-exclusion chromatography and x-ray diffraction of extracted and thermally deconstructed cellulose. DMAc-DMSO SEC **(A)** demonstrates that cellulose DP is slightly reduced in the early moments of thermal deconstruction. Additionally, x-ray diffraction (XRD) **(B)** indicates that cellulose crystallinity remains mostly intact after brief heating. Note: these results were generated using Sigmacell Type 50 cellulose, not red oak biomass.

other biopolymers. Hemicelluloses, represented by xylan, galactan, arabinan, mannan, and acetyl, decompose readily during thermal deconstruction. Notably, for hardwoods such as red oak, the galactan, arabinan, and mannan exist primarily within the innermost cell wall layers Holtzapple and Caballero, (2003). The extent to which these components volatilize demonstrates that, despite their brevity, reactions occurring during truncated thermal deconstruction experiments occur throughout the cell wall.

The native and residual lignin was determined using heteronuclear single-quantum coherence (HSQC) nuclear magnetic resonance (NMR) spectroscopy, which interrogates ^{1}H and ^{13}C nuclei, to determine how the various units decompose and monomers volatilize (Figure 6A). Similar experiments have been performed for low temperature biomass pretreatment processes and high temperature *ex situ* lignin analysis Kim et al. (2013); Yelle et al. (2013); Kim et al. (2014); Mittal et al. (2017a); Mittal et al. (2017b), but these data are the first obtained from whole plant cell wall materials from intermediate stages of rapid thermal deconstruction. The experiments revealed that even during truncated thermal deconstruction the structure of lignin was significantly modified.

Figures 6B, C were produced by taking relative abundance and accounting for respective yields of the solid biomass following the truncated thermal deconstruction.

Figure 6B demonstrates how certain lignin units, namely the β-ether unit (with its characteristic β–O–4 bond), decompose readily, whereas more recalcitrant sections remain unperturbed, including those units linked by β–β and β–5 bonds. Note that 5-5- and β-1 linked units were minor (<1%), as generally found for such high-S materials, and therefore not factored into the analysis. This result corroborates prior computational chemistry work that determined lignin bond dissociation energies (BDEs). The BDE of the β–O–4 bond (Parthasarathi et al., 2011) is less than that of either the β–β (Parthasarathi et al., 2011) or β–5. (Elder, 2014). This work

confirms deductions inspired by the results of computational chemistry studies Parthasarathi et al. (2011); Schutyser et al. (2018).

Additionally, the data in Figure 6C suggests avenues for future study. Guaiacyl and syringyl monomers decreased by at most 53% and 40% respectively; however, the α-keto-syringyl units S′ that arise primarily as artifacts of ball-milling were not reduced significantly. In biological processes, syringyl units **S** can be benzyl-oxidized to S′ units and a similar process may occur here, despite reaction in an inert gaseous environment. Regardless of the cause, this result indicates that monomers evolve from biomass at different relative rates.

Thermal deconstruction of cellulose cannot be investigated in the same manner as for hemicellulose or lignin. As a homopolymer, cellulose does not have different monomer and bond types to analyze. Instead, extracted cellulose (commercially available Sigmacell Type 50) was thermally deconstructed with the free fall reactor under similar conditions as the red oak. The resulting material was converted into anhydro-oligosaccharides via solid-phase reactions, confirmed by prior water-based size-exclusion chromatography (SEC) as described by Lindstrom et al. (2019b) and electron microscopy (see Supplemental Material).

Additionally, most of the thermally deconstructed cellulose did not dissolve in water, so dimethylacetamide (DMAc) with 8% lithium chloride (LiCl) (29, 30) was used to completely solubilize these samples (as well as extracted cellulose and the polysaccharide standards). The samples were then diluted with dimethyl sulfoxide (DMSO), which was used as the mobile phase for SEC. The DMAc-DMSO SEC found that water-insoluble anhydro-oligosaccharides are up to two orders of magnitude longer than their water-soluble counterparts. The weight average DP of each thermally deconstructed sample was approximately 20 times larger than has been previously reported from prior work using high heating rates Lindstrom et al. (2019b); Broido et al. (1973). Figure 7A shows the
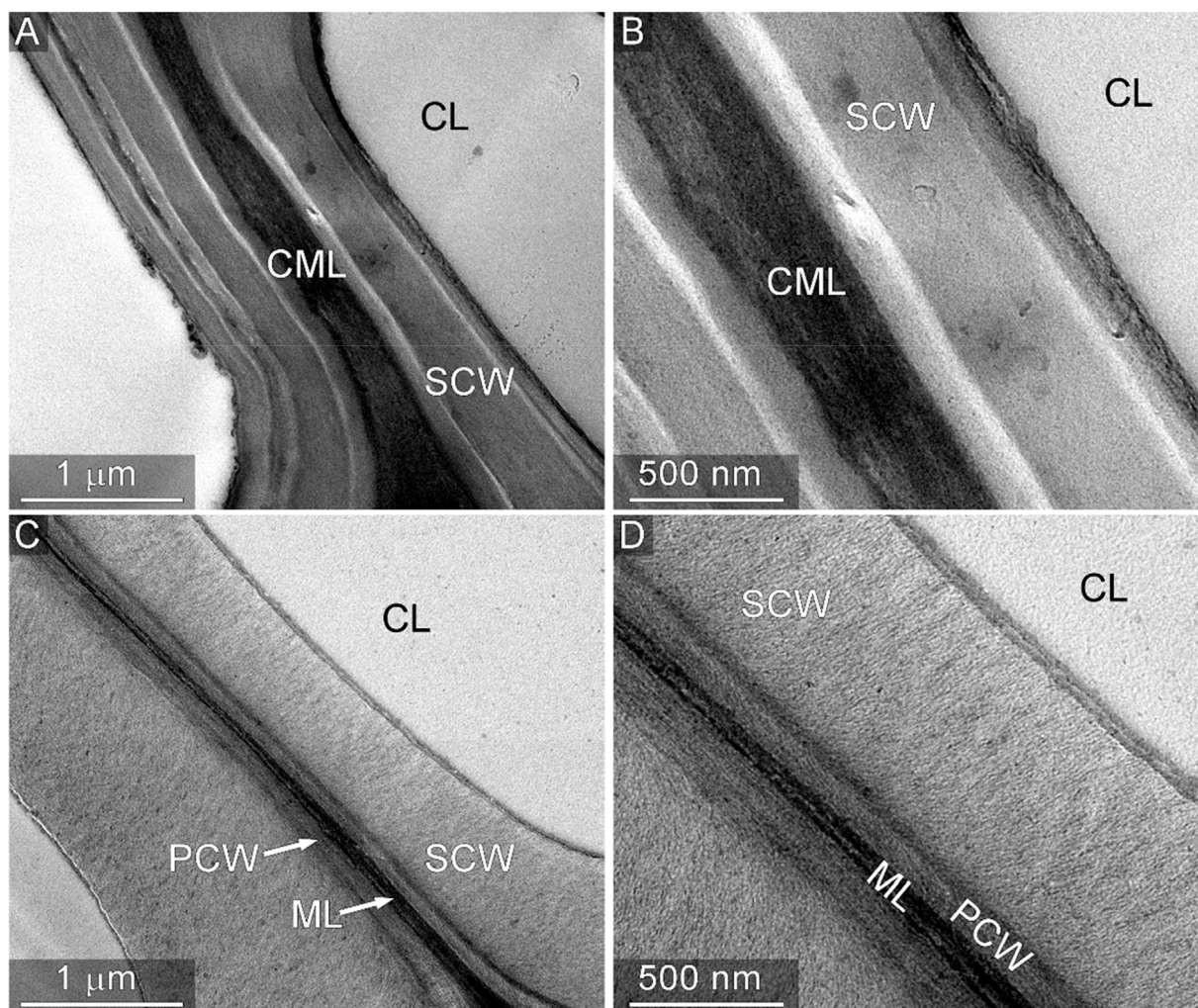
FIGURE 8
Transmission electron microscopy of native and thermally deconstructed cell walls. Micrographs of native cell wall thin sections stained with KMnO$_4$ are shown at two different magnifications in **(A)** and **(B)**. Micrographs of thermally deconstructed material subjected to identical sample preparation are shown in **(C)** and **(D)**. The lighter staining of the SCW and middle lamella region indicate a reduction in the lignin content relative to native material. Annotations: CL, cell lumen; CML, compound middle lamella; SCW, secondary cell wall; PCW, primary cell wall; ML, middle lamella.

quantified SEC results of these large anhydro-oligosaccharides and the cellulose control. Even in this early stage of thermal depolymerization the DP decreased by approximately 18%.

The chromatography validates the relative recalcitrance of cellulose compared to hemicellulose and lignin. X-ray diffraction (XRD) further confirms how little the cellulose was affected by the brief thermal deconstruction (Figure 7B). The cellulose crystallinity index decreases by 9, 7, and 16% during the approximately 1 s residence time of cellulose in the free fall reactor at reactor temperatures of 375, 400, and 450°C, respectively.

4 Cell wall structural degradation

Using transmission and scanning electron microscopy (denoted TEM and SEM, respectively), the biomass cell wall was probed for alterations in the ultrastructure. Figure 8 compares TEM micrographs at two different magnifications of thin sections of native and thermally deconstructed red oak. The samples were subjected to identical staining procedures using potassium permanganate (KMnO$_4$), which shows preference for lignin, Donohoe et al. (2012) to enhance contrast. As expected, the staining patterns of native cell walls (Figures 8A, B) displayed a lignin-rich compound middle lamella (CML), comprising the middle lamella and both primary cell walls from the adjoining cells, which stained darker than the adjacent layers of secondary cell wall (SCW). The thermally deconstructed samples (Figures 7C, D) exhibited a markedly different staining patterns. Furthermore, the staining of the SCWs was also lighter than observed for the native material. The reduction in staining intensity corroborates compositional analysis, indicating significant delignification occurs throughout the cell wall, and may be localized to regions of the cell wall that are relatively rich in the more volatile biopolymer components. Additionally, the texture of the thermally deconstructed material exhibited a prominent fibrillar pattern, further signifying lignin and hemicellulose removal.
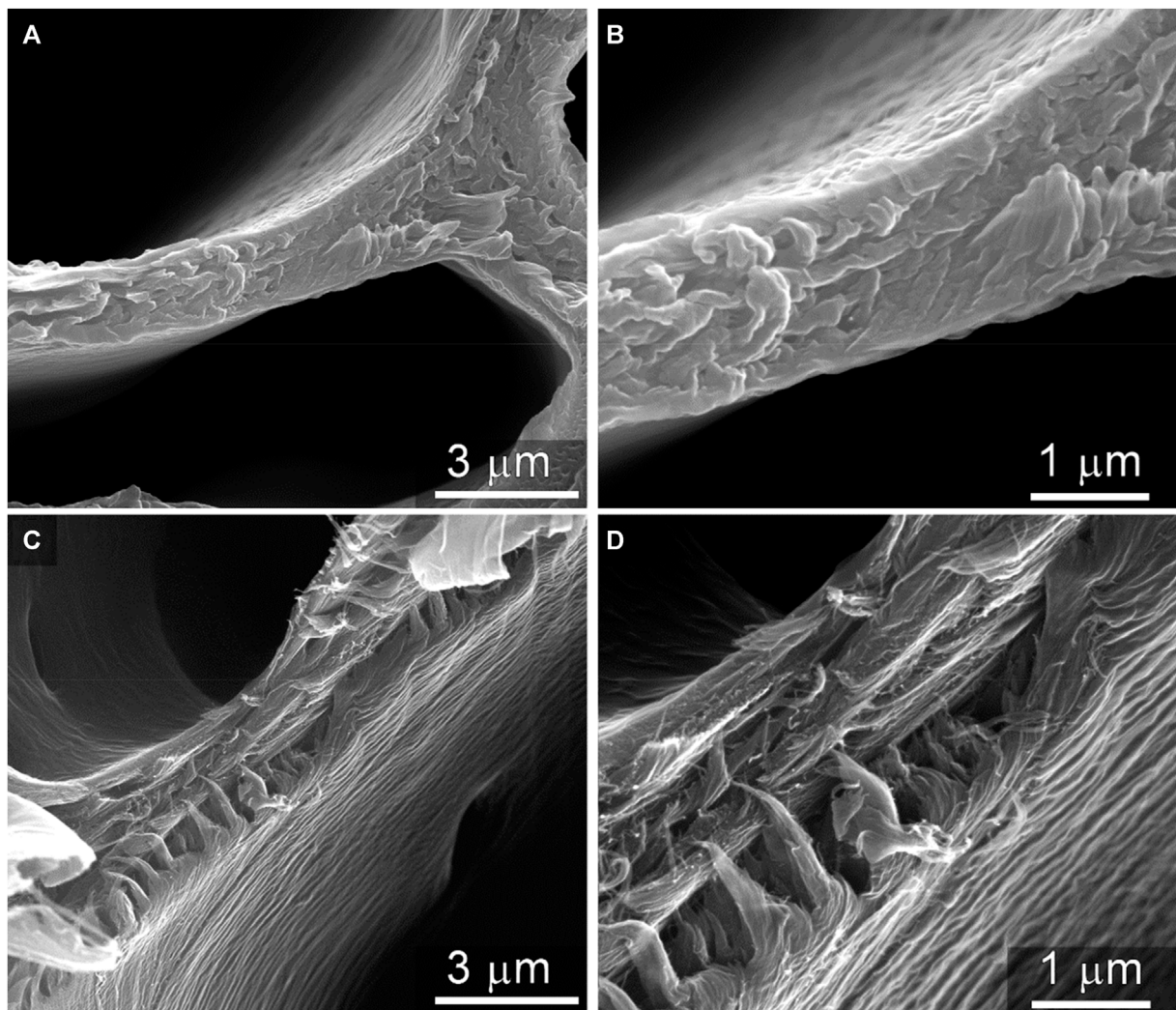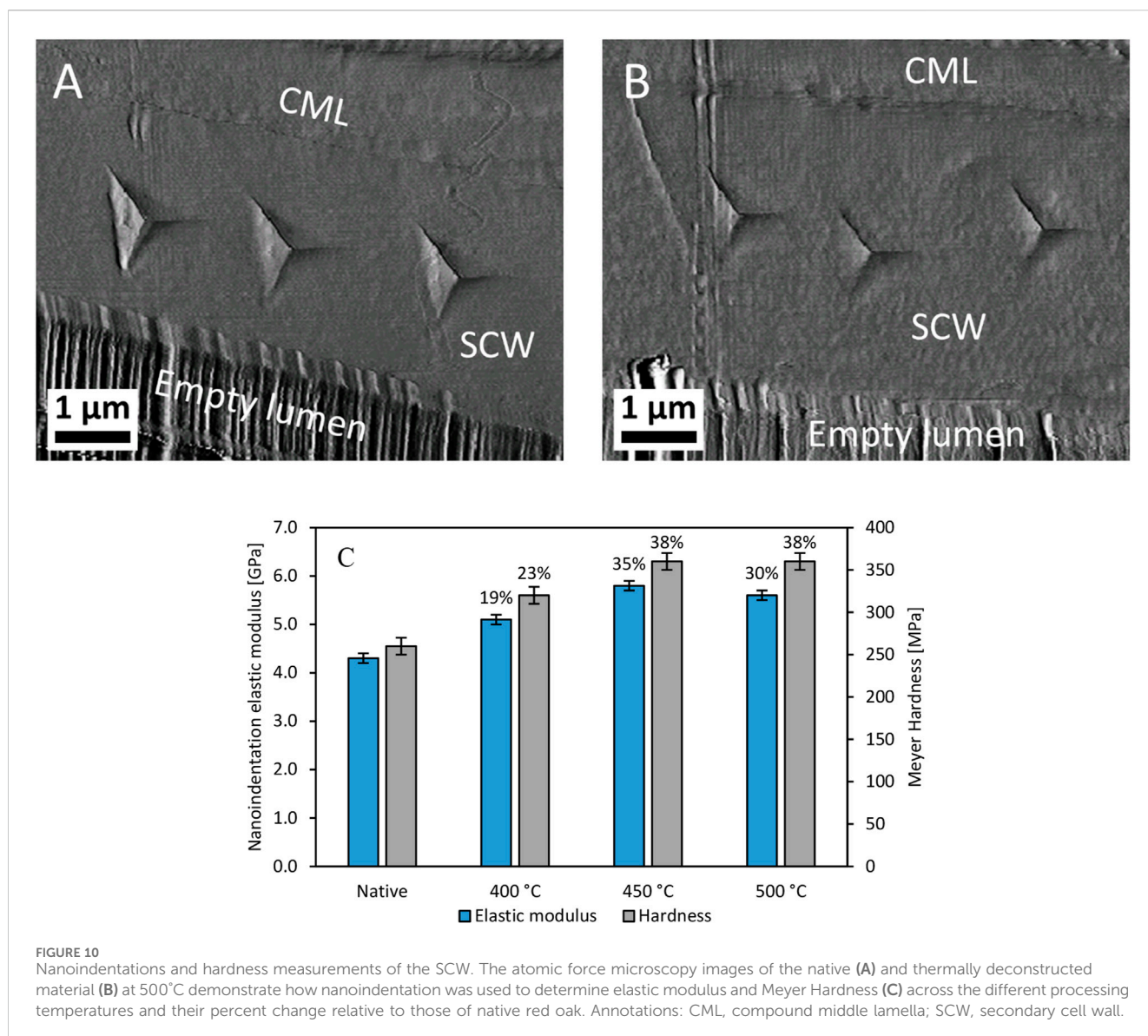
FIGURE 9
Scanning electron microscopy of native and thermally deconstructed cell walls. Micrographs of native cell wall cross sections are shown at two different magnifications in **(A)** and **(B)**. The cross-sectional surface of the thermally deconstructed material at two different magnifications in **(C)** and **(D)** display more fibrillar textures, which is characteristic of the nanostructure of cellulose microfibrils. This observation further supports the selective removal of the matrixing biopolymers lignin and hemicelluloses by the thermal deconstruction process.

SEM imaging was employed to provide complimentary structural information about the surface of the cell wall cross sections of the same samples. The morphology of the cleaved surface of native cell walls (Figures 9A, B) appeared globular, wherein bundles of cellulose fibrils are closely integrated with the cell wall matrix biopolymers, lignin and hemicellulose. In contrast, the morphology of the cleaved surface of the thermally deconstructed cell walls (Figures 9C, D) displayed a notably more detailed texture; the fibrillar structure of cellulose microfibrils can be clearly observed (particularly in Figure 9D). Similar features have been reported previously for the nanostructure of cellulose fibrils in maize SCWs after minor thermochemical pretreatments that remove and relocate lignin Ciesielski et al. (2013); Ciesielski et al. (2014). In the context of the study, these observations further support the selective removal of the matrixing biopolymers that ensconce the cellulose in the native material, leaving behind the cellulosic component in greater relative abundance and allowing for

clearer observation of its fibrillar nanostructure in the images of the thermally deconstructed material.

5 Cell wall mechanical properties

Nanoindentation was utilized to test SCW mechanical properties in the wood particles. The anatomical longitudinal plane was chosen because elastic modulus measurements are more sensitive to changes in matrix biopolymers when the elastic stiffness is measured perpendicular to the long axis of the stiff cellulose microfibrils. Nanoindentations were placed in SCWs between compound middle lamella and exposed lumina (Figures 10A, B). The noticeably smaller residual nanoindentation impressions in the thermally deconstructed specimen was the first indication that the thermally degraded SCWs increased in hardness, which indicates an increase in resistance to plastic

FIGURE 10
Nanoindentations and hardness measurements of the SCW. The atomic force microscopy images of the native **(A)** and thermally deconstructed material **(B)** at 500°C demonstrate how nanoindentation was used to determine elastic modulus and Meyer Hardness **(C)** across the different processing temperatures and their percent change relative to those of native red oak. Annotations: CML, compound middle lamella; SCW, secondary cell wall.

deformation. Quantifying the changes in hardness and nanoindentation elastic modulus for the native and thermally deconstructed material (Figure 10C) showed that thermal degradation modifies the SCWs inside the wood particles, corroborating the TEM and SEM observations (Figure 8; Figure 9).

The nanoindentation elastic modulus and hardness of the SCWs inside the particles increased after thermal deconstruction. Considering that the experiments were performed under 50% relative humidity conditions, the increased mechanical strength was likely caused by a reduction in water sorption capacity. Water acts as a plasticizer in SCWs, and nanoindentation measurements of mechanical properties in the transverse (Yu et al., 2011; Bertinetti et al., 2015) and longitudinal planes (Youssefian et al., 2017) of the SCW generally decrease with increasing amounts of absorbed water. Water sorption into hemicelluloses accounts for the majority of water sorption in SCWs Youssefian et al. (2017). Therefore, the increases in SCW mechanical properties with temperature support that hemicelluloses are being modified or removed from the thermally deconstructed

specimens. In previous nanoindentation experiments on the transverse wood plane, SCW hardness also increased in wood that underwent slow pyrolysis Zickler et al. (2006); Stanzl-Tschegg et al. (2009). Collectively, these results suggest that, although matrix biopolymers are being removed during thermal degradation, any potential formation of a porous structure was not sufficient to decrease the mechanical properties of the SCW.

6 Conclusion

By interrogating the solid-phase reactions that occur during biomass thermal deconstruction, measurements were possible that previous studies could only deduce. This work corroborates some prior theories but also adds substantial new insights. Primarily, these experiments indicated significant multiscale degradation stemming from underlying chemical transformations.

Cellulose, due to its insular microfibrils, resists initial thermal deconstruction more than does either hemicellulose or lignin.

Cellulose microfibrils are more intact than the surrounding hemicellulose and lignin, which has the effect of enriching biomass with cellulose temporarily—a phenomenon not previously anticipated or detected.

Hemicellulose, the other main class of biomass polysaccharides, rapidly decomposed as expected. Even under the brief reaction conditions, biomass hardness increased as hemicellulose was removed, corroborating related studies with substantially longer reaction durations Zickler et al. (2006); Stanzl-Tschegg et al. (2009).

Lignin contains bonds that vary in both strength and abundance, and these aspects greatly influence its deconstruction rate and products. In particular, lignin monomers volatilize at differing rates related to the initial composition of the lignin.

This study forays into the direct interrogation of solid-phase reactions during rapid thermal deconstruction of biomass particles. This multiscale investigation demonstrates that small chemical transformations can affect the larger physical structure and mechanical properties of biomass. Each length-scale is worth studying in whole plant cell wall materials, as many of these observations would not have been possible using extracted biopolymers. Overall, the rarely studied solid-phase reactions within biomass thermochemical processing are more varied than previously recognized, challenging models and theories to account for these phenomena.

7 Methods

7.1 Free-fall reactor

A free-fall reactor was used to generate thermally deconstructed red oak as described by Gable and Brown Gable and Brown (2016). Biomass was fed into a 3.05 m tall reactor tube made of 316L stainless steel (internal diameter of 0.035 m) heated by ceramic Wallow heaters. Three reactor temperatures were used for red oak: 400, 450, heated by ceramic Wallow heater and 500°C. The 450°C test was performed twice to collect sufficient solids for analysis, which is why error is displayed for the product yields. For cellulose (Sigmacell Type 50), three reactor temperatures were also used: 375, 400, 450°C. As estimated by modeling in the Supplemental Material, after approximately 0.9 s of residence time, the reacting particles exited the reactor tube at temperatures below the reactor temperature and were rapidly quenched with gaseous nitrogen at approximately −196°C, stopping all reactions promptly.

This method allows the effect of different temperatures to be compared directly by only changing the thermal profile experienced by the particles. (Red oak final particle temperatures and residence times predicted by computational fluid dynamics are contained in Supplemental Material.) The vapor or aerosol products were collected by an electrostatic precipitator and then a condenser. The non-condensable gas yield was determined by difference.

7.2 Ultimate, proximate, and compositional analyses

A Mettler Toledo thermogravimetric analyzer (TGA)/ differential scanning calorimeter (DSC) was used to determine the amount of moisture, volatiles, fixed carbon, and ash in each substrate using a 20 ± 0.5 mg sample. These tests were conducted in duplicate. The temperature profile used was developed by Johnston Johnston (2017).

An Elementar vario MICRO cube elemental analyzer was used to quantify chemical elements. Carbon, hydrogen, nitrogen, and sulfur content was determined, whereas oxygen was calculated by difference Johnston, (2017). These tests were conducted in duplicate.

The compositional analysis was performed at the National Renewable Energy Laboratory using standard laboratory analysis procedures for ash, Sluiter et al. (2008) lignin, Sluiter et al. (2012) structural carbohydrates, Sluiter et al. (2012) and extractives content.

7.3 HSQC NMR

Gel-state whole-cell-wall HSQC was performed on a Bruker Biospin AVANCE-III 700 MHz spectrometer following the procedure described by Kim and Ralph Kim and Ralph (2010). Briefly, the coarsely-ground biomass (0.5 g) was either used as is or solvent extracted sequentially with distilled water and 80% ethanol (each using ultrasonication, 1 h, three times), then ball-milled using a Fritsch Planetary micro mill Pulverisette 7 vibrating at 600 rpm for 4 h. The ball-milled sample (50 mg) was dissolved into DMSO-d_6/pyridine-d_5 (0.6 mL, 4:1, v/v) and subjected to HSQC studies. Bruker's Topspin 3.5 pL 7 (Mac) software was used to process spectra. The central DMSO solvent peak was used as internal reference (δ_C 39.5, δ_H 2.49 ppm).

7.4 Size-exclusion chromatography

The cellulose, thermally deconstructed cellulose, and Pullulan polysaccharide standards (Agilent Technologies), were dissolved in dimethylacetamide (DMAc) with 8% LiCl using the procedure described in McCormick McCormick (1981). The dissolved samples were then diluted with DMSO to match the 0.5% LiCl concentration in the mobile phase in accordance with Schult et al. Schult et al. (2002).

A Dionex UltiMate® 3000 HPLC (high performance liquid chromatography) was used with a Shodex refractive index (RI) detector and Chromeleon® software. A PolyPore guard column (50 × 7.5 mm) and two PolyPore SEC columns (300 × 7.5 mm) from Agilent Technologies were used in series. The column temperature was held at 70°C with a flow rate of 0.4 mL min^{-1}. DMSO was used as the mobile phase.

The Pullulan polysaccharide standards with the following peak molecular weights [Da] were used to calibrate the SEC: 6,100; 9,600; 21,100; 47,100; 107,000; 200,000; 344,000; and 708,000.

7.5 X-ray diffraction

The cellulose and thermally deconstructed cellulose samples were analyzed by a Siemens D500 x-ray diffractometer using the

procedure described in the supplemental material from Zhang et al. Zhang et al. (2014).

7.6 Transmission electron microscopy

Samples were dehydrated by treating with increasing concentrations of ethanol in a Pelco laboratory microwave oven. Samples were then infiltrated with LR White (London Resin Company) at room temperature overnight. The infiltrated samples were polymerized in an oven in a nitrogen environment at 60°C overnight. Samples were sectioned to ~80 nm and collected on polyvinyl formal coated copper slot grids (SPI Supplies, West Chester, PA). Grids were post-stained for 1 min with 1% aqueous $KMnO_4$. Images were captured with a four-megapixel Gatan UltraScan 1000 CCD camera (Gatan, Pleasanton, CA) using FEI Tecnai G2 20 Twin LaB6 TEM operated at 200 kV accelerating voltage (FEI, Hillsboro, OR).

7.7 Scanning electron microscopy

Samples were hand-sectioned to reveal cross sections of xylem tissue. The sections were freeze-dried prior to imaging to avoid dehydration artifacts and then mounted on aluminum stubs using carbon tape. The mounted samples were sputter-coated with 8 nm of iridium. Imaging was performed at beam accelerating voltages from 15 to 20 keV with a FEI Quanta 400 FEG scanning electron microscope (FEI, Hillsboro, OR).

7.8 Nanoindentation

For the native and thermally deconstructed red oak, a representative wood particle was chosen. Nanoindentation surfaces were prepared in the longitudinal plane of unembedded wood following previously established procedures Jakes et al. (2008); Jakes et al. (2009a); Jakes et al. (2015). Quasi-static, multiload nanoindentation experiments were performed using a Bruker-Hysitron (Minneapolis, Minnesota, United States) TriboIndenter® equipped with a Berkovich probe. The relative humidity (RH) inside of the nanoindentation enclosure was maintained at 50% using an InstruQuest (Coconut Creek, Florida, United States) HumiSys™ HF RH generator. Prepared specimens were placed inside of the nanoindenter enclosure at least 60 h before experiment commencement, and the RH was maintained during the experiments. In each specimen, five to eight nanoindentations were performed in three different cell walls. The multiload nanoindentations were analyzed using the structural compliance method to correct for any potential edge effects and specimen-scale flexing Jakes et al. (2008); Jakes et al. (2009b). Elastic modulus and Meyer hardness values were then calculated. A Quesant (Agoura Hills, California, United States) atomic force microscope (AFM) incorporated in the TriboIndenter was used for high resolution imaging or residual nanoindentations. The AFM was operated in contact mode and calibrated in lateral directions using an Advanced Surface Microscopy (Indianapolis, Indiana, United States) calibration standard as described previously Jakes et al. (2008)..

Data availability statement

The original contributions presented in the study are included in the article/Supplementary materials, further inquiries can be directed to the corresponding author.

Author contributions

JL: Formal Analysis, Writing–original draft. CP: Formal Analysis, Investigation, Writing–original draft. PC: Formal Analysis, Investigation, Writing–original draft. JR: Formal Analysis, Funding acquisition, Writing–review and editing. MC: Formal Analysis, Investigation, Writing–original draft. JJ: Formal Analysis, Investigation, Writing–review and editing. PJ: Formal Analysis, Methodology, Writing–original draft. SR: Formal Analysis, Investigation, Methodology, Writing–review and editing. RB: Conceptualization, Funding acquisition, Writing–review and editing.

Funding

Acknowledgments

Conflict of interest

The authors declare that the research was conducted in the absence of any commercial or financial relationships that could be construed as a potential conflict of interest.

Publisher's note

All claims expressed in this article are solely those of the authors and do not necessarily represent those of their affiliated organizations, or those of the publisher, the editors and the reviewers. Any product that may be evaluated in this article, or claim that may be made by its manufacturer, is not guaranteed or endorsed by the publisher.

References

Bertinetti, L., Hangen, U. D., Eder, M., Leibner, P., Fratzl, P., and Zlotnikov, I. (2015). Characterizing moisture-dependent mechanical properties of organic materials: humidity-controlled static and dynamic nanoindentation of wood cell walls. *Philos. Mag.* 95, 1992–1998. doi:10.1080/14786435.2014.920544

Breault, R. W. (2010). Gasification processes old and new: a basic review of the major technologies. *Energies* 3, 216–240. doi:10.3390/en3020216

Bridgwater, A. V. (2012). Review of fast pyrolysis of biomass and product upgrading. *Biomass Bioenergy* 38, 68–94. doi:10.1016/j.biombioe.2011.01.048

Broido, A., Javier-Son, A. C., Ouano, A. C., and Barrall, E. M., II (1973). Molecular weight decrease in the early pyrolysis of crystalline and amorphous cellulose. *J. Appl. Polym. Sci.* 17, 3627–3635. doi:10.1002/app.1973.070171207

Ciesielski, P. N., Matthews, J. F., Tucker, M. P., Beckham, G. T., Crowley, M. F., Himmel, M. E., et al. (2013). 3D electron tomography of pretreated biomass informs atomic modeling of cellulose microfibrils. *ACS Nano* 7, 8011–8019. doi:10.1021/nn4031542

Ciesielski, P. N., Wang, W., Chen, X., Vinzant, T. B., Tucker, M. P., Decker, S. R., et al. (2014). Effect of mechanical disruption on the effectiveness of three reactors used for dilute acid pretreatment of corn stover Part 2: morphological and structural substrate analysis. *Biotechnol. Biofuels* 7, 47. doi:10.1186/1754-6834-7-47

Donohoe, B. S., Ciesielski, P. N., and Vinzant, T. B. (2012). "Preservation and preparation of lignocellulosic biomass samples for multi-scale microscopy analysis," in *Biomass conversion* (Totowa, NJ: Humana Press), 31–47.

Elder, T. (2014). Bond dissociation enthalpies of a pinoresinol lignin model compound. *Energy and Fuels* 28, 1175–1182. doi:10.1021/ef402310h

Evershed, R. P., Jerman, K., and Eglinton, G. (1985). Pine wood origin for pitch from the Mary Rose. *Nature* 314, 528–530. doi:10.1038/314528a0

Gable, P., and Brown, R. C. (2016). Effect of biomass heating time on bio-oil yields in a free fall fast pyrolysis reactor. *Fuel* 166, 361–366. doi:10.1016/j.fuel.2015.10.073

Ghosh, A., and Haverly, M. R. (2019). "Solvent liquefaction," in *Thermochemical processing of biomass: conversion into fuels, chemicals and power*. Editor R. C Brown. ed. 2 (John Wiley and Sons), 257–306.

Gowlett, J. A. J. (2016). The discovery of fire by humans: a long and convoluted process. *Philosophical Trans. R. Soc. B Biol. Sci.* 371, 20150164. doi:10.1098/rstb.2015.0164

Holtzapple, M. T. (2003). "Hemicelluloses," in *Encyclopedia of food sciences and nutrition*. Editor B Caballero. ed. 2 (Elsevier), 3060–3071.

Iisa, K., Robichaud, D. J., Watson, M. J., ten Dam, J., Dutta, A., Mukarakate, C., et al. (2018). Improving biomass pyrolysis economics by integrating vapor and liquid phase upgrading. *Green Chem.* 20, 567–582. doi:10.1039/c7gc02947k

Jakes, J. E., Frihart, C. R., Beecher, J. F., Moon, R. J., Resto, P. J., Melgarejo, Z. H., et al. (2009b). Nanoindentation near the edge. *J. Mater. Res.* 24, 1016–1031. doi:10.1557/jmr.2009.0076

Jakes, J. E., Frihart, C. R., Beecher, J. F., Moon, R. J., and Stone, D. S. (2008). Experimental method to account for structural compliance in nanoindentation measurements. *J. Mater. Res.* 23, 1113–1127. doi:10.1557/jmr.2008.0131

Jakes, J. E., Hunt, C. G., Yelle, D. J., Lorenz, L., Hirth, K., Gleber, S.-C., et al. (2015). Synchrotron-based X-ray fluorescence microscopy in conjunction with nanoindentation to study molecular-scale interactions of phenol–formaldehyde in wood cell walls. *ACS Appl. Mater. Interfaces* 7, 6584–6589. doi:10.1021/am5087598

Jakes, J. E., Yelle, D. J., Beecher, J. F., Frihart, C. R., and Stone, D. S. (2009a). "Characterizing polymeric methylene diphenyl diisocyanate reactions with wood: 2. nanoindentation," in *International conference on wood Adhesives*. Editors C. R. Frihart, C. G. Hunt, and R. J. Moon (Lake Tahoe, Nevada, USA: Forest Products Society), 366–374.

Johnston, P. A. (2017), Iowa State University. thesis.

Kim, H., and Ralph, J. (2010). Solution-state 2D NMR of ball-milled plant cell wall gels in DMSO-d6/pyridine-d5. *Org. Biomol. Chem.* 8, 576–591. doi:10.1039/b916070a

Kim, J.-Y., Hwang, H., Oh, S., Kim, Y.-S., Kim, U.-J., and Choi, J. W. (2014). Investigation of structural modification and thermal characteristics of lignin after heat treatment. *Int. J. Biol. Macromol.* 66, 57–65. doi:10.1016/j.ijbiomac.2014.02.013

Kim, J. Y., Oh, S., Hwang, H., Kim, U. J., and Choi, J. W. (2013). Structural features and thermal degradation properties of various lignin macromolecules obtained from poplar wood (Populus albaglandulosa). *Polym. Degrad. Stab.* 98, 1671–1678. doi:10.1016/j.polymdegradstab.2013.06.008

Koller, J., Baumer, U., Kaup, Y., and Weser, U. (2005). Herodotus' and Pliny's embalming materials identified on ancient Egyptian mummies. *Archaeometry* 47, 609–628. doi:10.1111/j.1475-4754.2005.00222.x

Lillebø, A. H., Holmen, A., Enger, B. C., and Blekkan, E. A. (2013). *Fischer-Tropsch conversion of biomass-derived synthesis gas to liquid fuels*, 2. Wiley Interdisciplinary Reviews: Energy and Environment, 507–524.

Lindstrom, J. K., Proano-Aviles, J., Johnston, P. A., Peterson, C. A., Stansell, J. S., and Brown, R. C. (2019b). Competing reactions limit levoglucosan yield during fast pyrolysis of cellulose. *Green Chem.* 21, 178–186. doi:10.1039/c8gc03461c

Lindstrom, J. K., Shaw, A., Zhang, X., and Brown, R. C. (2019a). "Condensed phase reactions during thermal deconstruction," in *Thermochemical processing of biomass: conversion to fuels, chemicals and power*. Editor R. C Brown. 2nd (John Wiley and Sons), 17–48.

Mandø, M. (2013). "Direct combustion of biomass," in *Biomass combustion science, Technology and engineering* (Elsevier), 61–83.

McCormick, C. L. (1981). Novel cellulose solutions.

Mittal, A., Katahira, R., Donohoe, B. S., Black, B. A., Pattathil, S., Stringer, J. M., et al. (2017a). Alkaline peroxide delignification of corn stover. *ACS Sustain. Chem. Eng.* 5, 6310–6321. doi:10.1021/acssuschemeng.7b01424

Mittal, A., Katahira, R., Donohoe, B. S., Pattathil, S., Kandemkavil, S., Reed, M. L., et al. (2017b). Ammonia pretreatment of corn stover enables facile lignin extraction. *ACS Sustain. Chem. Eng.* 5, 2544–2561. doi:10.1021/acssuschemeng.6b02892

Parthasarathi, R., Romero, R. A., Redondo, A., and Gnanakaran, S. (2011). Theoretical study of the remarkably diverse linkages in lignin. *J. Phys. Chem. Lett.* 2, 2660–2666. doi:10.1021/jz201201q

Schult, T., Hjerde, T., Optun, O. I., Kleppe, P. J., and Moe, S. (2002). Characterization of cellulose by SEC-MALLS. *Cellulose* 9, 149–158. doi:10.1023/a:1020139409903

Schutyser, W., Renders, T., Van den Bosch, S., Koelewijn, S.-F., Beckham, G. T., and Sels, B. F. (2018). Chemicals from lignin: an interplay of lignocellulose fractionation, depolymerisation, and upgrading. *Chem. Soc. Rev.* 47, 852–908. doi:10.1039/c7cs00566k

Shanks, B. H., and Keeling, P. L. (2017). Bioprivileged molecules: creating value from biomass. *Green Chem.* 19, 3177–3185. doi:10.1039/c7gc00296c

Sikarwar, V. S., Zhao, M., Clough, P., Yao, J., Zhong, X., Memon, M. Z., et al. (2016). An overview of advances in biomass gasification. *Energy and Environ. Sci.* 9, 2939–2977. doi:10.1039/c6ee00935b

Sluiter, A., Hames, B., Ruiz, R., Scarlata, C., Sluiter, J., and Templeton, D. (2008). Determination of ash in biomass. Golden, CO, United States. NREL/TP-510-42619

Sluiter, A., Hames, B., Ruiz, R., Scarlata, C., Sluiter, J., Templeton, D., et al. (2012). Determination of structural carbohydrates and lignin in biomass. Golden, CO, United States. NREL/TP-510-42618.

Stanzl-Tschegg, S., Beikircher, W., and Loidl, D. (2009). Comparison of mechanical properties of thermally modified wood at growth ring and cell wall level by means of instrumented indentation tests. *Holzforschung* 63, 443–448. doi:10.1515/hf.2009.085

Thompson, L. C., Ciesielski, P. N., Jarvis, M. W., Mukarakate, C., Nimlos, M. R., and Donohoe, B. S. (2017). Estimating the temperature experienced by biomass particles during fast pyrolysis using microscopic analysis of biochars. *Energy and Fuels* 31, 8193–8201. doi:10.1021/acs.energyfuels.7b00791

Tumuluru, J. S., Sokhansanj, S., Hess, J. R., Wright, C. T., and Boardman, R. D. (2011). REVIEW: a review on biomass torrefaction process and product properties for energy applications. *Ind. Biotechnol.* 7, 384–401. doi:10.1089/ind.2011.7.384

Weber, K., and Quicker, P. (2018). Properties of biochar. *Fuel* 217, 240–261. doi:10.1016/j.fuel.2017.12.054

Yelle, D. J., Kaparaju, P., Hunt, C. G., Hirth, K., Kim, H., Ralph, J., et al. (2013). Two-dimensional NMR evidence for cleavage of lignin and xylan substituents in wheat straw through hydrothermal pretreatment and enzymatic hydrolysis. *BioEnergy Res.* 6, 211–221. doi:10.1007/s12155-012-9247-6

Youssefian, S., Jakes, J. E., and Rahbar, N. (2017). Variation of nanostructures, molecular interactions, and anisotropic elastic moduli of lignocellulosic cell walls with moisture. *Sci. Rep.* 7, 2054. doi:10.1038/s41598-017-02288-w

Yu, Y., Fei, B., Wang, H., and Tian, G. (2011). Longitudinal mechanical properties of cell wall of Masson pine (Pinus massoniana Lamb) as related to moisture content: a nanoindentation study. *Holzforschung* 65, 121–126. doi:10.1515/hf.2011.014

Zhang, J., Nolte, M. W., and Shanks, B. H. (2014). Investigation of primary reactions and secondary effects from the pyrolysis of different celluloses. *ACS Sustain. Chem. Eng.* 2, 2820–2830. doi:10.1021/sc500592v

Zhang, X., and Brown, R. C. (2019). "Introduction to thermochemical processing of biomass into fuels, chemicals, and power," in *Thermochemical processing of biomass: conversion into fuels, chemicals and power*. Editor R. C Brown. ed. 2 (John Wiley and Sons), 1–16.

Zhu, C., Krumm, C., Facas, G. G., Neurock, M., and Dauenhauer, P. J. (2017). Energetics of cellulose and cyclodextrin glycosidic bond cleavage. *React. Chem. Eng.* 2, 201–214. doi:10.1039/c6re00176a

Zickler, G. A., Schöberl, T., and Paris, O. (2006). Mechanical properties of pyrolysed wood: a nanoindentation study. *Philos. Mag.* 86, 1373–1386. doi:10.1080/14786430500431390